chemistry

MDPI

Article

Conversion of Ethanol to Butadiene over Binary MgO-SiO_2 Mixed Oxides Prepared by the Ammonia Evaporation Method

Ismail Bin Samsudin, Stephan Jaenicke and Gaik-Khuan Chuah *

Department of Chemistry, National University of Singapore, 3 Science Drive 3, Kent Ridge, Singapore 117543, Singapore
* Correspondence: chmcgk@nus.edu.sg; Tel.: +65-65162839

Abstract: The ammonia evaporation method, originally applied for the preparation of highly dispersed silica-supported copper catalysts, was used to synthesize magnesia-silica for the one-step conversion of ethanol to 1,3-butadiene. The MgO-SiO_2 catalysts obtained by this method contained a high fraction of magnesium silicate hydrates, which are associated with enhanced butadiene selectivity. These catalysts were benchmarked against those prepared by a conventional wet-kneading method. A Mg/Si molar ratio of 4 was optimal, forming butadiene with 37% yield, which is far superior to the 15% yield obtained with MgO-SiO_2 formed by wet-kneading. At 475 °C and a WHSV of 3.2 h^{-1}, a productivity of 0.612 g_{BD} $g_{cat}{}^{-1}$ h^{-1} was measured without the catalyst suffering from deactivation, even after 52 h TOS. The catalysts were characterized by spectroscopic and thermal techniques to elucidate their physicochemical properties and explain the differences in the catalytic performance. The presence of magnesium silicate hydrates gave a balance of surface acidity and basicity, which greatly improved butadiene formation. The open morphology of MgO-SiO_2 with vertically arranged platelets and the presence of large pores are proposed to contribute to the stability of the catalyst.

Keywords: ethanol; butadiene; heterogeneous catalysis; acid-base; biomass

Citation: Samsudin, I.B.; Jaenicke, S.; Chuah, G.-K. Conversion of Ethanol to Butadiene over Binary MgO-SiO_2 Mixed Oxides Prepared by the Ammonia Evaporation Method. *Chemistry* **2023**, *5*, 544–558. https://doi.org/10.3390/chemistry5010039

Academic Editors: José Antonio Odriozola and Hermenegildo García

Received: 1 February 2023
Revised: 3 March 2023
Accepted: 5 March 2023
Published: 7 March 2023

1. Introduction

Increasing concerns over the depletion of petroleum feedstocks have expedited the search for renewable resources and sustainable processes [1–3]. 1,3-Butadiene (BD) is an important chemical in the manufacture of synthetic rubbers and elastomers [4–6]. Currently, over 95% of BD is obtained as a side product of the ethylene steam cracking process [7,8]. However, the shift from naphtha to natural gas as feed for the ethylene crackers in recent years has impacted the availability of BD, such that production is no longer sufficient to meet market demand [9–11]. This puts bioethanol in focus as a feedstock for BD production given its ready availability, with up to 52 million tonnes being produced in the USA alone in 2018 [12–18]. Interestingly, the Lebedev process to obtain butadiene from ethanol was already used at an industrial scale in the 1930s. This process used magnesia-silica catalysts. Subsequent studies showed that the composition and preparation methods of the catalysts strongly affected performance. A Mg/Si ratio > 1 is necessary for high selectivity to BD, although the reported optimum ratios vary widely [19–21]. Various methods have been disclosed for the synthesis of magnesia-silica, e.g., sol-gel processing, wet-kneading, impregnation and co-precipitation, which results in catalysts with significantly different physical and chemical properties [22–25]. Catalysts prepared by the sol-gel, wet-kneading and impregnation methods gave BD yields between 20–24% at weight hourly space velocity (WHSV) between 0.4–2.4 h^{-1} [19,26,27]. In contrast, much lower yields of only ~6% were obtained with catalysts synthesized by co-precipitation [28]. Angelici et al. observed that BD yield decreased for catalysts prepared by wet-kneading > co-precipitation > physical mixture [28,29]. These variations were attributed to differences in the morphology and

acid-base properties of the materials. Co-precipitated samples contained both more acidic and more strong basic sites than the wet-kneaded samples; these sites favour the formation of ethylene and diethyl ether instead of BD. The choice of the magnesium salt as a precursor also plays a role in the wet-kneading process [30–32]. Magnesium hydroxide, either commercially obtained or freshly precipitated from $Mg(NO_3)_2$, is preferred. In a published study, MgO gave similar catalytic activity as $Mg(OH)_2$ but the use of $MgCl_2$ resulted in poorer BD selectivity [32].

The presence of magnesium silicates in MgO-SiO_2 has been shown to be important for butadiene formation [24,31]. Using ^{1}H-^{29}Si CP-MAS NMR, Chung et al. identified different types of anhydrous, amorphous hydrous and layered hydrous magnesium silicate in wet-kneaded MgO-SiO_2 [26]. These silicates differ in the concentration and strength of their acid and/or basic sites. High BD yield was found to correlate with the layered magnesium silicate hydrates (lizardite, stevensite and talc), suggesting that these are the catalytically relevant species. The formation of layered magnesium silicate hydrates (MSH) from the dissolution of silicic acid, $Si(OH)_4$, in the basic MgO solution, has been widely studied in the cement industry [26,33,34]. Temuujin et al. found that the water of hydration in silicic acid is important, as hardly any layered magnesium silicate hydrate was formed when silica gel was used [35]. Clearly, the choice of preparation parameters is very important, as it affects the composition and performance of the MgO-SiO_2 catalysts. Since freshly created surfaces appear to be more amendable to the formation of magnesium silicate hydrates, we rationalized that ammonia evaporation could be a useful approach. In this methodology, typically used to form highly dispersed metals on silica, ammonia is added to complex the metal ions. Subsequent evaporation of the ammonia leads to a decrease of the pH, accompanied by hydrolysis of the metal-ammonia complex [36–42]. We reasoned that at the initial high pH, the surface of the silica particles dissolves to form silicic acid, which reacts with dissolved $Mg(OH)_2$. The intimate mixing in the homogeneous solution facilitates the formation of magnesium silicate hydrates as the ammonia is driven off and the pH falls from 11 to 8. The effect of using the ammonia evaporation synthesis on the morphology, acid-base properties, and the amount and nature of magnesium silicates is compared with MgO-SiO_2 produced by wet-kneading. In this way, the structure and performance of the ammonia-evaporated MgO-SiO_2 catalysts for ethanol-to-butadiene transformation can be rationally assessed.

2. Materials and Methods

2.1. Chemicals

SiO_2 was obtained from PQ Corporation, while MgO and $Mg(NO_3)_2{\cdot}6H_2O$ were supplied by Sigma Aldrich. 28% ammonia solution was purchased from VWR Chemicals. The chemicals were of analytical grade and used as received.

2.2. Catalyst Preparation

In a typical ammonia evaporation (AE) synthesis for MgO-SiO_2 (molar ratio 4), 4.256 g $Mg(NO_3)_2{\cdot}6H_2O$ and 0.25 g SiO_2 were added to 200 mL aqueous 1 M NH_4OH. After stirring for 4 h at room temperature, the mixture was brought to 80 °C and held at this temperature for 3 h to completely evaporate the ammonia. The solid was recovered by filtration, dried at 80 °C overnight, washed with deionized water and calcined at 500 °C for 6 h. MgO-SiO_2 with Mg/Si molar ratio of 1, 2, 5 and 10 were similarly prepared and are referred to as MgO-SiO_2-*n* where *n* refers to the Mg/Si ratio. For comparison, a MgO-SiO_2 sample with Mg/Si ratio of 4 was also synthesized by wet-kneading (WK). MgO and SiO_2 were suspended in deionized water (ratio of water/solid (g/g) = 100) and stirred at room temperature for 7 h. The solid was recovered by filtration and treated as described for the ammonia-evaporated samples.

2.3. Catalyst Characterisation

Powder X-ray diffraction (XRD) patterns were obtained using a Bruker (Karlsruhe, Germany) D8 Advance diffractometer (40 kV, 40 mA) equipped with a copper anode ($\lambda_{K\alpha1}$ = 1.5406 Å) and a LynxEye XE detector. The spectra were recorded over a 2θ range from 5 to 80° using a step size of 0.02° and a dwell time of 0.5 s/step with the samples spun at 30 rpm. Nitrogen isotherms were measured on a Micromeritics (Norcross, GA, USA)) Tristar 3000 after degassing the samples under nitrogen flow at 300 °C for 10 h. The pore size distributions were obtained from the desorption isotherms using the Barrett-Joyner-Halenda (BJH) method. Fourier transform infrared spectroscopy (FTIR) measurements were taken with a Bruker Alpha FTIR (Karlsruhe, Germany) spectrometer. The acidity of the samples was determined by temperature-programmed desorption (TPD) of ammonia. Each sample was pretreated at 500 °C for 2 h under a flow of He. It was then allowed to cool to 100 °C and exposed to a flow of ammonia for 15 min. The sample was then flushed with He for 1 h before the temperature was raised to 550 °C at 10 °C min^{-1} and the desorbing ammonia was monitored by a Balzers Prisma 200 quadrupole mass spectrometer (Asslar, Germany). The basicity of samples was similarly determined by TPD of carbon dioxide following adsorption at 25 °C. Electron micrographs were obtained using a JEOL (Tokyo, Japan) JSM-6701F (SEM) and a JEOL JEM-3010 (TEM). ^{29}Si MAS NMR spectra were measured on a Bruker AVNEO-400 (Karlsruhe, Germany) wide bore solid-state spectrometer operating at 79.49 MHz with a spinning rate of 10 kHz, pulse width of 4 μs and recycle delay of 10 s. The samples were packed into 4 mm zirconia rotors and the ^{29}Si chemical shifts are reported relative to a TMS standard. XPS was performed on a VG-Scientific ESCALAB Mark 2 (East Grinstead, UK) spectrometer equipped with a hemispherical electron analyser and a Mg K_α anode (1253.6 eV) at 300 W. The C 1s signal of adventitious carbon at 285 eV was used as reference. The abundance of the various species was quantified from the peak areas, with appropriate correction for the atomic sensitivity factors. Elemental analysis was performed by ICP-AES (Perkin Elmer Avio 500, Waltham, MA, USA) after dissolution of the samples in HF/HNO_3.

2.4. Catalytic Activity

A fixed-bed gas phase continuous flow reaction system was used for catalytic testing. 0.1 g MgO-SiO_2 catalyst and 1.5 g glass beads (180 μm, Sigma-Aldrich, St. Louis, MO, USA) were placed in a tubular glass reactor fitted with a fritted disk (i.d. 10 mm). The catalyst was pretreated in He at 400 °C for 1 h, before feeding ethanol at a rate of 400 μL/h with a syringe pump into the He carrier gas flow at 55 mL/min. The temperature was varied from 400 to 475 °C. The effluent was detected by an online gas chromatograph (HP 5890 series II) using an FID detector. The products were verified by GC-MS. Weight hourly space velocity (WHSV), gas hourly space velocity (GHSV) and productivity were calculated as follows:

$$WHSV\left(h^{-1}\right) = \frac{Mass\ of\ ethanol\ feed\ per\ hour}{Mass\ of\ catalyst} \quad (1)$$

$$GHSV\left(h^{-1}\right) = \frac{Volume\ of\ ethanol\ feed\ per\ hour}{Volume\ of\ reactor} \quad (2)$$

$$Productivity\left(\frac{g(butadiene)}{g(catalyst)\cdot h}\right) = \frac{Mass\ of\ butadiene\ formed\ per\ hour}{Mass\ of\ catalyst} \quad (3)$$

3. Results and Discussion

3.1. Textural Properties of MgO-SiO_2

A series of MgO-SiO_2 with varying Mg/Si ratios from 1 to 10 were prepared by ammonia evaporation. The SiO_2 used in catalyst preparation was mesoporous with a surface area of 423 m^2/g, but the 500 °C-calcined MgO-SiO_2 samples had smaller surface areas and pore volumes (Table 1). The surface areas decreased with higher MgO content (from 281 to 87 m^2/g). The MgO-SiO_2 sample prepared by wet-kneading (Mg/Si molar

ratio of 4) had significantly different textural properties. The surface area was higher (178 vs. 142 m^2/g), but the pore volume smaller (0.35 vs. 0.96 cm^3/g) than that of the ammonia-evaporated MgO-SiO_2 sample. Nitrogen porosimetry showed that the pores in the wet kneaded MgO-SiO_2-4 were narrowly distributed around ~3.8 nm, with a smaller density of wider pores from 5 to 45 nm (Figure S1 from Supplementary Materials). On the other hand, the pores in the ammonia-evaporated MgO-SiO_2-4 were bigger and broadly distributed between 5–50 nm. ICP-AES measurements confirmed that the Mg and Si content of all the samples closely correlated with the starting composition.

Table 1. Physicochemical properties of MgO-SiO_2 catalysts prepared by ammonia evaporation and wet-kneading (WK).

Sample	Surf. Area (m^2/g)	Micropore Area (m^2/g)	Pore Vol. (cm^3/g)	Mg/Si [a]
MgO-SiO_2-1	281	32	0.61	0.96
MgO-SiO_2-2	206	35	0.70	2.03
MgO-SiO_2-4	142	41	0.96	3.97
MgO-SiO_2-5	127	43	0.83	4.91
MgO-SiO_2-10	87	9	0.38	9.87
MgO-SiO_2-4 (WK)	178	49	0.35	3.94
MgO	59	0	0.17	-
SiO_2	423	30	2.41	-

[a] Mg/Si molar ratios were determined by ICP-AES.

The X-ray diffractograms of the 80 °C-dried samples synthesized by the ammonia evaporation method showed that crystalline $Mg(OH)_2$ (brucite) was present (Figure 1a). Irrespective of the Mg/Si ratio, no diffraction peaks of crystalline SiO_2 phases could be detected, which can be attributed to its amorphous nature. During calcination at 500 °C, the $Mg(OH)_2$ dehydrated to form MgO (periclase) (Figure 1b). This is clearly reflected in the FTIR spectra, which show the appearance of Mg-O bands (865 and 1466 cm^{-1}) at the expense of the Mg-OH band (3700 cm^{-1}) (Figure S2 from Supplementary Materials). In the X-ray diffractograms, new broad peaks appear at 2θ ~ 35–39° and 58–62°, which can be assigned to magnesium silicate hydrates (MSH) [43]. These hydrates are formed after calcination at 500 °C and remain stable up to 800 °C. However, after heating to 900 °C, the XRD pattern shows a mixture of MgO, $MgSiO_3$ (enstatite) and Mg_2SiO_4 (fosterite) (Figure 1c). The crystalline magnesium silicates ($MgSiO_3$ and Mg_2SiO_4) are formed by dehydration of magnesium silicate hydrates; their amount can be correlated to the fraction of amorphous hydrates originally present [44]. In contrast, the XRD pattern of the sample obtained by wet-kneading indicates that MgO is partially hydrolysed to $Mg(OH)_2$ (Figure 1d). After calcination at 500 °C, MgO, magnesium silicate hydrates and a small amount of $MgSiO_3$ identified from the weak diffraction peak at 2θ ~ 37° was present. The narrower linewidth of the MgO peaks indicates that the crystallites are bigger in the wet-kneaded sample. Using the Scherrer equation, the crystallite size of MgO was calculated to be 17.9 nm for the wet-kneaded MgO-SiO_2 whereas it was only 6.6 nm in ammonia-evaporated samples. After further heating to 900 °C, the sample contained predominantly MgO, with a much smaller content of $MgSiO_3$ and Mg_2SiO_4. Thus, it can be inferred that wet-kneading forms significantly less magnesium silicate hydrates than ammonia evaporation.

From the SEM micrographs, it can be seen that the initial silica comprised aggregates of various sizes in the micron range (Figure S3a,b from Supplementary Materials). Following ammonia evaporation, the surface of the SiO_2 aggregates became increasingly covered with platelets of MgO (Figure S3c–j from Supplementary Materials), such that above Mg/Si = 4, distinct regions of SiO_2 could no longer be discerned. Interestingly, these platelets grew out of the SiO_2 surface, as confirmed by elemental maps, which show the presence of both Mg and Si (Figure S4 from Supplementary Materials). This is clearly seen for MgO-SiO_2-4 where the perpendicular orientation of the MgO platelets gives a distinct floret-like appearance to the composite (Figure 2a,b). In contrast, the SEM images of the wet-kneaded MgO-SiO_2-4

show multiple layers of MgO platelets lying flat atop the silica particles (Figure 2d,e). The TEM micrographs are consistent with the distinctively different orientation of the MgO platelets on SiO_2 for the two samples (Figure 2c,f).

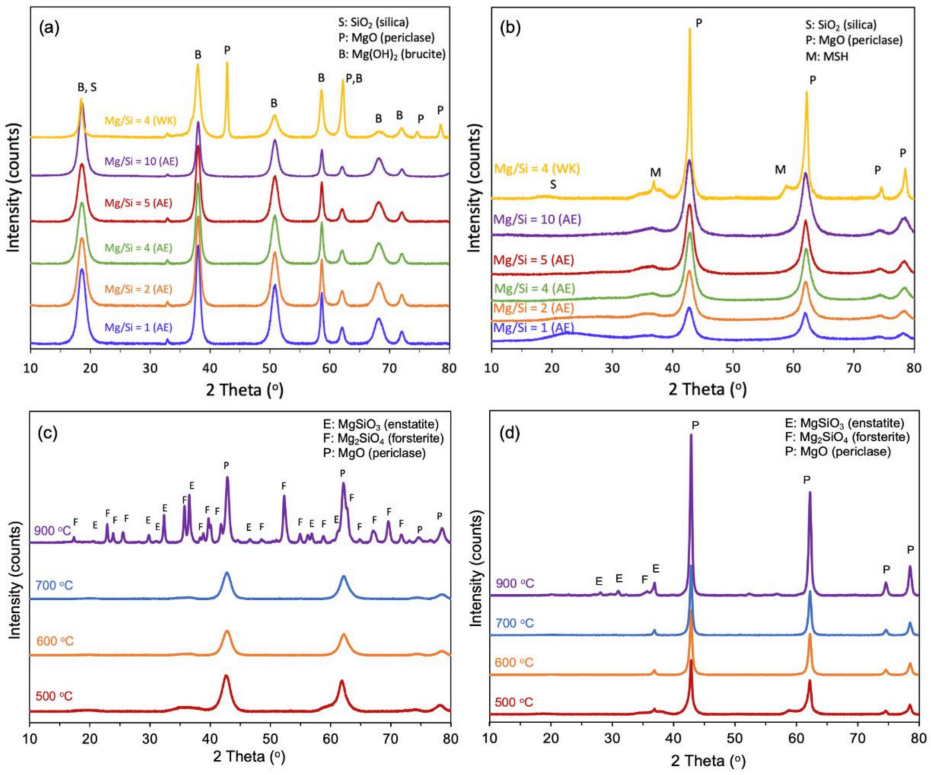

Figure 1. XRD of ammonia-evaporated (AE) MgO-SiO_2 with different Mg/Si loadings and of wet-kneaded (WK) MgO-SiO_2-4 after (**a**) drying at 80 °C and (**b**) calcination at 500 °C (**c**) MgO-SiO_2-4 (AE) and (**d**) MgO-SiO_2-4 (WK) after calcination at various temperatures.

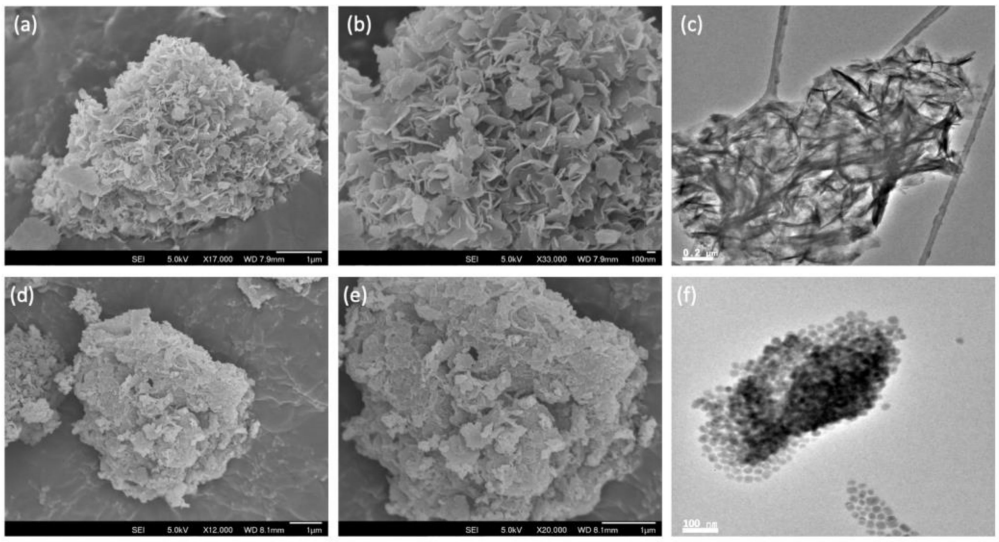

Figure 2. SEM and TEM images of SiO_2-MgO catalysts prepared by the (**a**–**c**) ammonia evaporation and (**d**–**f**) wet-kneading methods.

Solid-state ^{29}Si NMR measurements were performed to gain more information on the extent of magnesium silicate formation in MgO-SiO_2-4 prepared by ammonia evaporation and wet-kneading. The ^{29}Si-MAS NMR spectra could be deconvoluted into a number of

peaks representative of silicon in different environments from Q^1 to Q^4, where Q^n denotes the number of nearest Si atoms in $Si(OSi)_n(OMg)_{4-n}$ (Figure 3). The peaks at −81, −86 and −94 ppm are assigned to Q^1, Q^2 and Q^3 silicon, and are therefore indicative of the presence of magnesium silicate hydrates [45–49]. In the wet-kneaded MgO-SiO_2-4, the Q^1 and Q^2 peaks are broader, which suggest that there is greater structural disorder in the magnesium silicate hydrates than in the ammonia-evaporated sample. The Q^3 peak at −94 ppm is typically found in the serpentine group of minerals, $Mg_3Si_2O(OH)_4$, which includes chrysotile, antigorite and lizardite [26,45]. From the deconvoluted peak areas, it can be seen that the Q^3 signal is the major component in the ammonia-evaporated MgO-SiO_2-4 (Figure 3b). In addition, two separate Q^4 peaks were observed; one at −104 ppm, which is assigned to $(SiO)_3$Si-OH, associated with Si at surface sites, and another at −113 ppm due to framework $(SiO)_4Si$ [49]. The presence of these Q^4 peaks shows that not all the silica reacted with magnesium to form magnesium silicate hydrates. The unreacted silica constituted a smaller fraction of the total signal in MgO-SiO_2 synthesized by ammonia evaporation than by wet-kneading (26% vs. 51%).

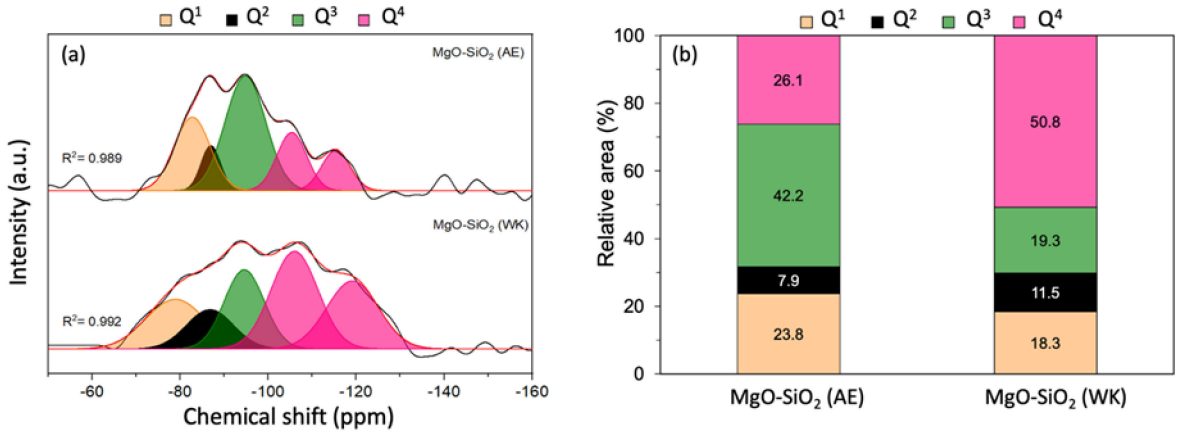

Figure 3. (**a**) ^{29}Si MAS NMR spectra of MgO-SiO_2 prepared by ammonia evaporation (AE) and wet-kneading (WK) and (**b**) relative areas of the Q^n signals.

The enhanced formation of magnesium silicate hydrates in the ammonia-evaporated MgO-SiO_2 suggests that the synthesis procedure promotes intimate contact between the substrates. This can be explained by the isoelectric points (IEP) of pH 2 and pH 12 for SiO_2 and $Mg(OH)_2$, respectively [26,50]. Under the basic synthesis conditions (from initial pH 11 to pH 8), the surface of SiO_2 will be negatively charged and will attract Mg^{2+} ions or positively charged colloidal $Mg(OH)_2$ particles. Dissolving $SiO_{4-x}^{(4-2x)-}$ anions react with the positively charged magnesium species to form magnesium silicates, which promote a close interface between SiO_2 and $Mg(OH)_2$.

3.2. Acid-Base Properties

Due to the multiple steps in the ETB reaction, a good balance of acidic and basic sites is important for an effective catalyst. TPD of NH_3 and CO_2 was carried out to quantify the acidity and basicity of the samples. The amounts of NH_3 that desorbed from MgO were negligible due to its basic nature, while the weakly acidic SiO_2 also shows only a small desorption peak (Figure S5a from Supplementary Materials). In contrast, NH_3 desorbed from the MgO-SiO_2 over a wide temperature range from 150 to ~400 °C. This is very different from the component oxides, showing that new acidic sites are created in the MgO-SiO_2. With higher Mg content (Mg/Si increasing from 1 to 10), the NH_3 desorption profiles became narrower due to loss of strong acid sites. Simultaneously, the total density of acid sites decreased from 447 to 213 µmol/g (Table S1 from Supplementary Materials). Figure 4a,b compare the TPD of NH_3 for ammonia-evaporated and wet-kneaded MgO-SiO_2-4. The total acidity was slightly higher for the wet-kneaded sample (362 µmol/g) than the ammonia

evaporated sample (305 µmol/g) (Table S2 from Supplementary Materials). Due to heterogeneity of sites, they were arbitrarily assigned to weak, medium and strong acid sites based on the temperature range for NH_3 desorption. Both catalysts had predominantly medium (desorption between 200 and 300 °C), followed by weak (100–200 °C) and strong acid sites (>300 °C). From the tailing to temperatures higher than 450 °C, it can be inferred that the wet-kneaded MgO-SiO_2 had stronger acid sites than the ammonia-evaporated sample.

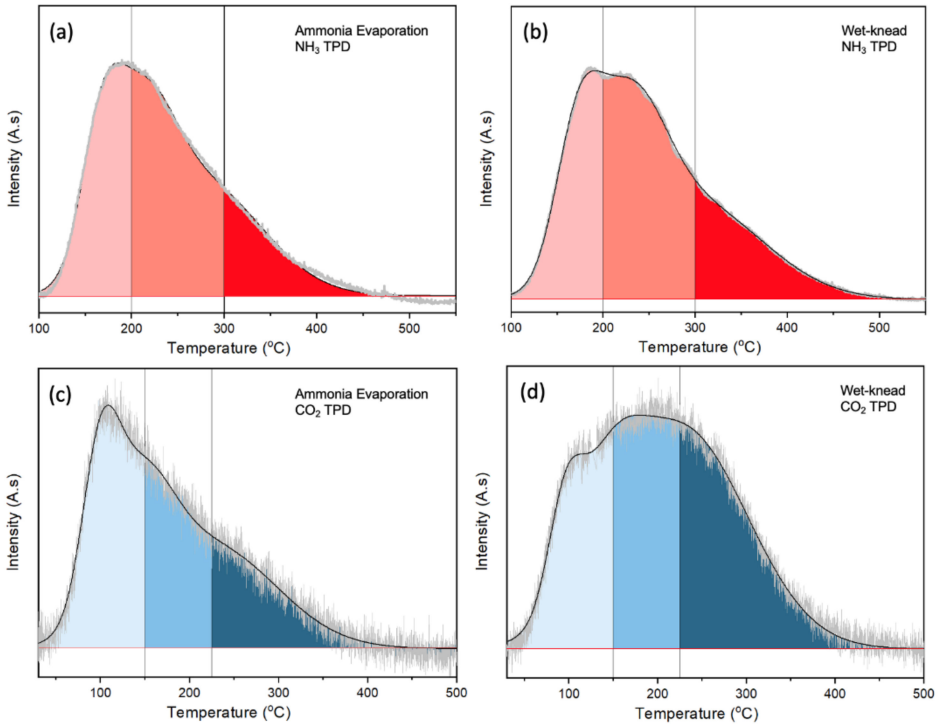

Figure 4. TPD of (**a**,**b**) NH_3 and (**c**,**d**) CO_2 over MgO-SiO_2-4 catalysts prepared by ammonia evaporation and wet-kneading.

The presence of basic sites in MgO-SiO_2 can be deduced from the CO_2 TPD where desorption occurred between 50 to 400 °C (Figure S5b from Supplementary Materials). Again, the sites were assigned to weak (<150 °C), medium (150–225 °C) and strong basicity (>225 °C). With increasing Mg/Si, more sites with higher basic strength were present. The total density of basic sites increased from 115 to 367 µmol/g for Mg/Si 1 to 10 (Table S1 from Supplementary Materials). Although MgO-SiO_2-4 synthesized by ammonia evaporation and wet-kneading have very similar densities of basic sites, ~290 µmol/g and 291 µmol/g, respectively, their CO_2 desorption profiles differ (Figure 4c,d). In the ammonia-evaporated MgO-SiO_2, the relative fraction of basic sites decreased from weak > medium > strong; the higher fraction of weak basic sites suggests modulation by the presence of SiO_2. The wet-kneaded sample had a higher proportion of medium and strong basic sites. Its similar desorption profile with that for MgO shows that there is less modulation by the presence of SiO_2, which suggests that SiO_2 and MgO exist as distinct phases.

The surface composition of MgO-SiO_2-4 was analysed using XPS (Figure 5). In the ammonia-evaporated sample, the Si 2p peak has very low intensity, which implies that there is little Si located at the surface, but rather it is buried within the bulk [51]. On the other hand, a strong Mg 2p peak is noted in agreement with the SEM images, which show the SiO_2 particles are covered by MgO platelets. The surface Mg/Si ratio was 17, which is much higher than the bulk Mg/Si ~ 4 determined by ICP-AES. In the wet-kneaded MgO-SiO_2-4, the Si 2p and Mg 2p peaks can be clearly discerned. The surface Mg/Si of 6.8 shows that the SiO_2 surface is not completely covered by MgO. The high surface area of SiO_2 (423 m^2/g) contributes significantly to the Si signal [52].

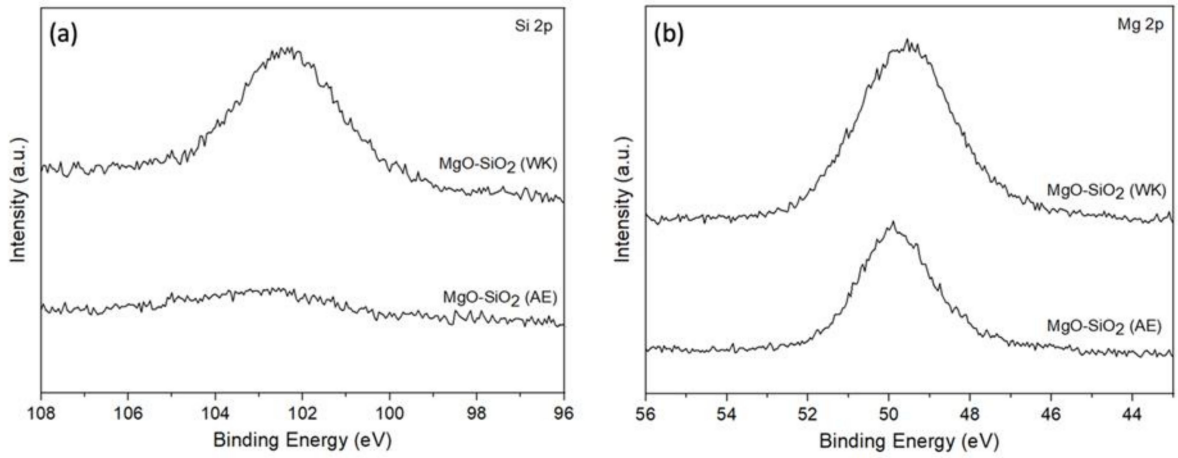

Figure 5. XPS spectra of the (**a**) Si 2p and (**b**) Mg 2p regions for MgO-SiO_2 prepared by ammonia evaporation (AE) and wet-kneading (WK).

3.3. Catalytic Activity for Ethanol to Butadiene (ETB)

Several mechanisms have been proposed for ethanol-to-butadiene (ETB) conversion over the years [53–56]. It is generally accepted that the reaction involves the following steps: (i) dehydrogenation of ethanol to acetaldehyde, (ii) aldol condensation of acetaldehyde to 3-hydroxybutanal (acetaldol), (iii) dehydration of 3-hydroxybutanal to crotonaldehyde, (iv) Meerwein-Ponndorf-Verley (MPV) reduction of crotonaldehyde by hydrogen transfer from ethanol to yield crotyl alcohol and (v) dehydration of crotyl alcohol to butadiene [57,58]. Depending on the acid/base properties of the catalysts, variable amounts of side products due to dehydration and/or condensation are formed. These include ethylene, butenes, diethyl ether, ethyl acetate, 1-butanol, hexadiene and hexatriene (Scheme 1).

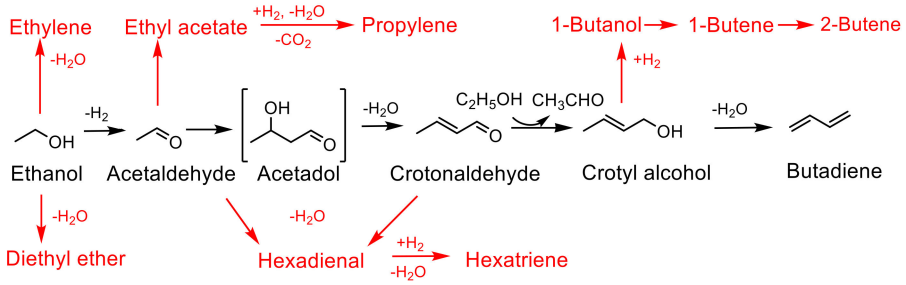

Scheme 1. Reaction pathway for ethanol to butadiene. The main pathway is shown in black with side products denoted in red.

3.3.1. Variation of Mg/Si Ratio, Reaction Temperature and Flow Rates

The catalytic performance of the MgO-SiO_2 catalysts with different Mg/Si ratios were tested for ethanol-to-butadiene conversion in a flow reactor. At 375 °C, ethanol conversion was between 26–52%, depending on the catalysts, and increased to >99% above 450 °C (Figure S6 from Supplementary Materials). The main products formed are ethylene, butadiene and acetaldehyde. Other side products including diethyl ether, butene, crotonaldehyde and butanol are formed in smaller amounts and are grouped under "others" in Figure 6. Over MgO-SiO_2-1 at 475 °C, ethylene made up 76.7% of the products, with butadiene being the second most major product at 15.3% (Figure 6a). This can be attributed to the high SiO_2 content as the presence of acidic sites favours the dehydration of ethanol to ethylene. With the increase in the Mg/Si ratio, more basic sites become available, which are catalytically active in hydrogen transfer reactions (e.g., dehydrogenation of ethanol and MPV of crotonaldehyde). Consequently, less ethylene and more acetaldehyde and

butadiene were formed. The highest butadiene selectivity, 26.8%, was observed for Mg/Si 4; at even higher Mg/Si, the butadiene selectivity was only 20–23%. Surprisingly, the decrease in butadiene selectivity over these Mg-rich catalysts was accompanied by more ethylene being formed. One reason could be that the nature of the magnesium silicate hydrates is dependent on varying Mg/Si ratios. Chung et al. showed that the presence of amorphous hydrous magnesium silicates correlated linearly with ethylene yield [26]. It is clear that a balance between acid and basic sites is required for the ETB reaction. Overall, the results revealed that the optimum combination of acidic and basic sites can be found in MgO-SiO_2-4.

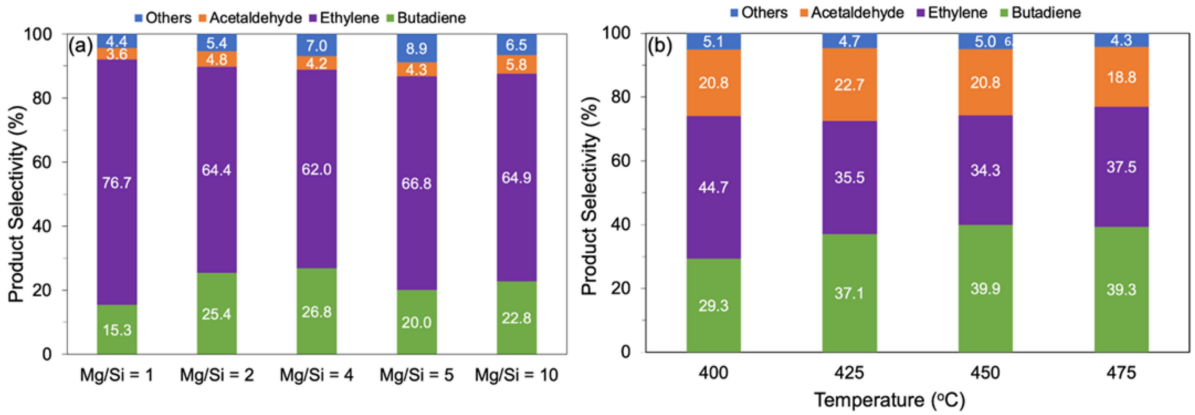

Figure 6. Product distribution (**a**) as function of composition over MgO-SiO_2 (AE) with different Mg/Si ratios at 475 °C and (**b**) as function of temperature over MgO-SiO_2-4 (AE). Reaction conditions: 0.1 g catalyst, 1.5 g glass beads, 55 mL/min He, time-on-stream = 4 h, ethanol concentration (**a**) 100 µL/h (3.2 vol%) and (**b**) 400 µL/h (11.3 vol%).

The temperature dependence of the reaction was studied at a higher ethanol concentration in the feed stream (11.3 vol%). At reaction temperatures > 400 °C, ethanol conversion was >90%. The product distribution depended on temperature. At 400 °C, ethylene was the main product, but its selectivity dropped, whereas the selectivity to acetaldehyde and butadiene increased as the temperature was increased to 475 °C (Figure 6b). The product selectivity changed most significantly from 400 to 425 °C, with only a slight improvement beyond this temperature with a butadiene selectivity of 37–39%.

The effect of ethanol flow rate (WHSV) was investigated for MgO-SiO_2-4 (AE) at 475 °C (Figure 7). When the ethanol concentration (vol%) was increased at constant He flow, the conversion decreased slightly from >99% at WHSV of 0.8 h^{-1} to 90% at WHSV of 3.2 h^{-1}; a further increase to 7.2 h^{-1} resulted in a steeper drop to 67.4%. However, the butadiene selectivity increased with increasing vol% ethanol in the feed and reached a plateau at about 39% for WHSV of 3.2 h^{-1} and higher. This WHSV corresponds to 11.3 vol% ethanol in the reactor and demonstrates the high turnover capacity of the catalyst. Next, the He flow rate was increased while maintaining ethanol at 11.3 vol% (Figure S7 from Supplementary Materials). A conversion > 95% was maintained up to a gas hourly space velocity (GHSV) of 3720 h^{-1} but decreased with higher GHSV. The butadiene selectivity increased with GHSV to a maximum of 39% at 3720 h^{-1} and decreased thereafter. At low GHSV, ethylene was the main product, but its selectivity decreased with increasing GHSV; in contrast, the selectivity to acetaldehyde increased with GHSV, showing that the successive steps to butadiene were affected by the shortened contact time.

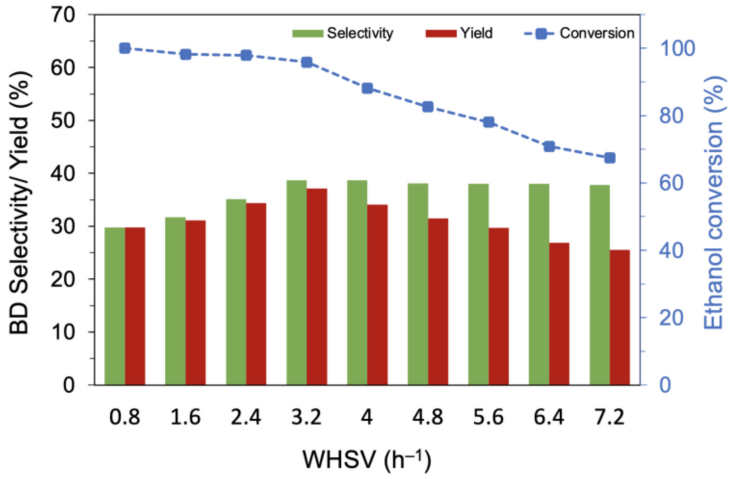

Figure 7. Variation of the butadiene selectivity and yield with ethanol flow rate over MgO-SiO_2-4 (AE). Reaction conditions: 0.1 g catalyst, 1.5 g glass beads, 475 °C and 55 mL/min He.

3.3.2. Effect of Synthesis Methods

The catalyst MgO-SiO_2 with Mg/Si 4, which showed the best activity, was compared with an identical composition synthesized by wet-kneading. At temperatures between 400 and 475 °C, the conversion was similar for both catalysts (Figure 8a). However, over the wet-kneaded MgO-SiO_2, ethylene formed as main product (70–73% selectivity), whereas over the ammonia-evaporated catalyst, much more butadiene and acetaldehyde were obtained. The butadiene yield was about 2.5 times higher than with the wet-kneaded sample, resulting in a productivity of 0.69 g_{BD} g_{cat}^{-1} h^{-1} (Figure 8b). This productivity is substantially higher than the benchmark of 0.15 g_{BD} g_{cat}^{-1} h^{-1} quoted as necessary for industrial relevance [59].

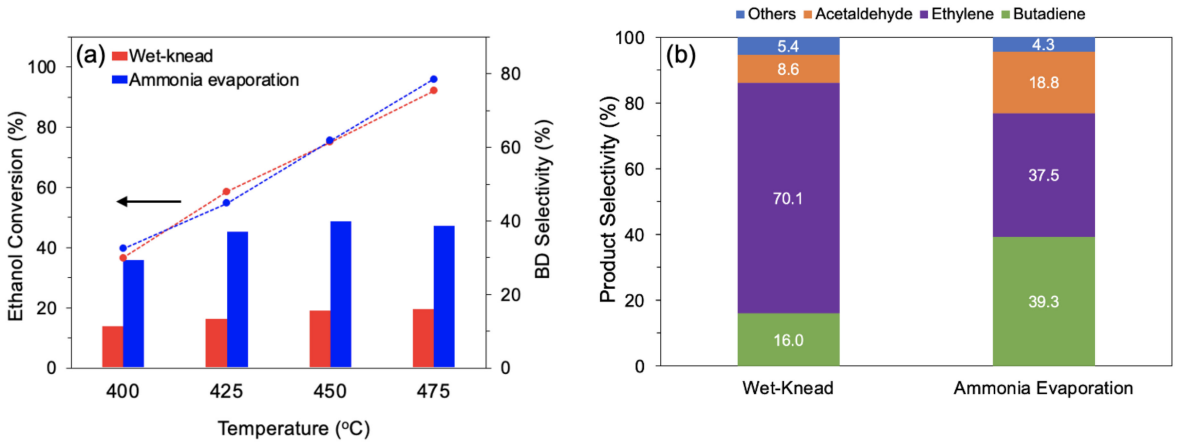

Figure 8. Comparison of MgO-SiO_2-4 prepared by wet-kneading and ammonia evaporation (**a**) ethanol conversion and butadiene selectivity at various temperatures and (**b**) product selectivity at 475 °C. Reaction conditions: 0.1 g catalyst, 1.5 g glass beads, 55 mL/min He, 400 µL/h ethanol (11.6 vol% ethanol), and TOS = 4 h.

The performance of the ammonia-evaporated catalyst compares well with other MgO-SiO_2 catalysts, where productivities of 0.027 to 1.00 g_{BD} g_{cat}^{-1} h^{-1} were reported (Table 2). The highest productivity of 1.00 g_{BD} g_{cat}^{-1} h^{-1} was observed for a wet-kneaded MgO-SiO_2 that had ultrathin MgO sheets arranged in a flower-like manner [60]. This morphology was postulated to enhance the catalytic activity. However, the productivity of this catalyst decreased to 0.67 g_{BD} g_{cat}^{-1} h^{-1} after 40 h on-stream. Another catalyst with comparable

activity was described by Reschetilowski et al., who found that a high MgO content of 85–95 mole% gave an optimum butadiene yield [24].

Table 2. Catalytic performance of $MgO\text{-}SiO_2$ catalysts.

Catalyst	T (°C)	Conv. (%)	BD Sel. (%)	BD Yield (%)	Productivity ($g_{BD}\ g_{cat}^{-1}\ h^{-1}$)	Ref
$MgO\text{-}SiO_2$-4 (AE)	475	96	39	37	0.69	This work
$MgO\text{-}SiO_2$-4 (WK)	475	94	16	15	0.27	This work
$MgO\text{-}SiO_2$ (WK)	325	35	44	15	0.027	[21]
$MgO\text{-}SiO_2$ (WK)	425	65	34	23	0.14	[26]
$MgO\text{-}SiO_2$ (WK) [a]	450	67	63	42	1.00	[60]
$MgO\text{-}SiO_2$ (WK) [b]	450	42	53	22	0.64	[24]
$MgO\text{-}SiO_2$ (Sol gel)	400	40	40	16	0.22	[19]
$MgO\text{-}SiO_2$ (Co-precipitate)	425	46	13	6	-	[28]
$MgO\text{-}SiO_2$ (Impregnation) [c]	350	81	30	24	0.056	[27]

[a] MgO with hierarchical flower-like nanostructure. [b] MgO platelets with secondary pore system. [c] Feed was a mixture of ethanol, acetaldehyde and water.

The acid-base properties lend insights into the nature of sites required for the multiple reaction steps and explain the different catalytic performance of the two catalysts. The lower selectivity to ethylene over the ammonia-evaporated $MgO\text{-}SiO_2$ can be attributed to the smaller density of strongly acidic sites (55 µmol/g) compared to the wet-kneaded sample (83 µmol/g). The bulk of the acid sites are of weak and medium strength, which is adequate for the dehydration of alkenols (e.g., crotyl alcohol) to butadiene. The CO_2 TPD showed that both catalysts contained basic sites, which are required to catalyze ethanol dehydrogenation to acetaldehyde and its subsequent aldol condensation [61,62]. Although the total density of basic sites is very similar for both samples, the ammonia-evaporated $MgO\text{-}SiO_2$ has mainly weak basic sites, whereas the wet-kneaded catalyst has predominantly medium-to-strong basic sites. Over the ammonia-evaporated $MgO\text{-}SiO_2$, the concentration of the reaction intermediate, acetaldehyde, was more than twice that of the wet-kneaded catalyst (18.8 vs. 8.6%). The accumulation of acetaldehyde indicates that the subsequent step (aldol condensation of acetaldehyde to acetaldol) requires sites of higher basic strength. However, the ammonia-evaporated catalyst gives a far better butadiene yield and much less ethylene. This can be attributed to its larger amount of magnesium silicate hydrates, as found by XRD and NMR studies described in Section 3.1. This agrees well with previous studies linking the presence of magnesium silicate hydrates to the selective formation of butadiene [22,26,63].

3.3.3. Stability of Ammonia-Evaporated $MgO\text{-}SiO_2$

Deactivation of catalysts in the ethanol-to-butadiene reaction is a common challenge and seems to be mostly caused by coke deposition [64,65]. For example, Zhang et al. reported that the total ethanol conversion over $MgO\text{-}SiO_2$ catalysts prepared by deposition-precipitation decreased from ~61 to 37% after only 5 h, and further to 23% after 30 h time-on-steam (TOS) [66]. In contrast, the ammonia-evaporated $MgO\text{-}SiO_2$-4 catalyst

exhibited excellent stability (Figure 9). Throughout the 52 h time-on-stream, the ethanol conversion and butadiene selectivity remained constant. The observed stability can be attributed to its large pore size and significant porosity, which mitigates the effects of coke deposition. The presence of large pores has been associated with increased stability of ETB catalysts [67]. SEM images of the used catalyst showed that the floret-like morphology was still present (Figure S8 from Supplementary Materials). After recalcination at 500 °C, subsequent testing found no significant change in its catalytic activity (Figure S9 from Supplementary Materials).

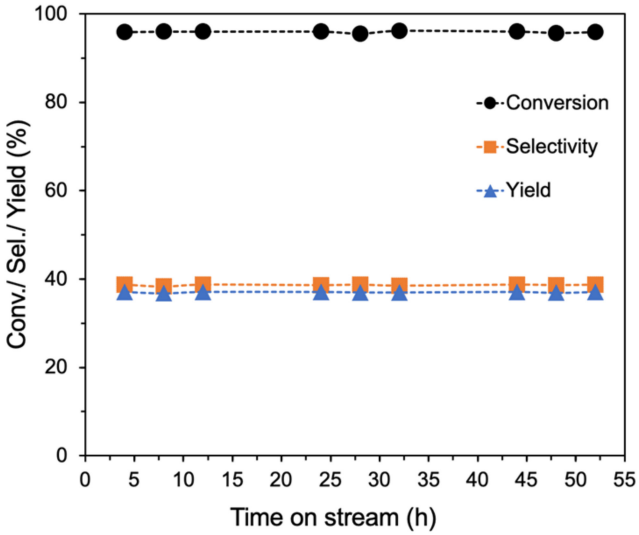

Figure 9. Stability studies of ammonia-evaporated MgO-SiO_2-4. Reaction conditions: 0.1 g catalyst, 1.5 g glass beads, 475 °C, 55 mL/min He and 400 µL/h ethanol (11.6 vol% ethanol).

4. Conclusions

A series of MgO-SiO_2 catalysts was synthesized using the ammonia evaporation method on the premise that the pH conditions during synthesis was more conducive to the formation of magnesium silicate hydrates through electrostatic interaction between the negatively charged siloxane groups at the silica surface and positively charged Mg^{2+} ions and colloidal $Mg(OH)_2$ particles. Characterization by XRD and solid-state ^{29}Si NMR confirmed that the content of magnesium silicate hydrates in the MgO-SiO_2 materials formed by ammonia evaporation was higher than for that synthesized by wet-kneading, a method that is known to give catalysts with good activity. The XRD patterns obtained after calcination at 900 °C showed that more $MgSiO_3$ and Mg_2SiO_4 were formed in the ammonia-evaporated MgO-SiO_2 than the wet-kneaded sample. A MgO-SiO_2 ratio of 4:1 gave the best catalytic performance for the ethanol-to-butadiene reaction, maintaining steady activity for 52 h on-stream. This may be due to its more open floret morphology, which facilitated access to active sites while having large pores made it more resistant to deactivation by coke deposition. Its butadiene selectivity (39%) was about 2.5 times higher than for an equivalent sample prepared by wet-kneading. Hence, the ammonia evaporation method is a promising synthesis strategy for preparing efficient catalysts for the ETB reaction.

Supplementary Materials: The following supporting information can be downloaded at: https://www.mdpi.com/article/10.3390/chemistry5010039/s1, Figure S1: (a) Nitrogen sorption isotherms and (b) pore size distributions of SiO_2-MgO-4 catalysts prepared by ammonia evaporation and wet-knead; Figure S2: FTIR of MgO-SiO_2 catalysts prepared by ammonia evaporation and wet-knead, before and after calcination at (a) low wavenumbers and (b) high wavenumbers; Figure S3: FESEM images of (a,b) SiO_2 and ammonia evaporated (c,d) MgO-SiO_2-0.5, (e,f) MgO-SiO_2-1, (g,h) MgO-SiO_2-4 and (i,j) MgO-SiO_2-10; Figure S4: SEM/EDS images of (a–d) MgO-SiO_2-0.5, (e–h) MgO-

SiO_2-1 (i–l) MgO-SiO_2-4 and (m–p) MgO-SiO_2-10; Figure S5: TPD of (a) NH_3 and (b) CO_2 over ammonia-evaporated MgO-SiO_2 catalysts, SiO_2 and MgO; Figure S6: (a) Ethanol conversion (b) BD selectivity and (c) BD yield for MgO-SiO_2 (AE) catalysts at varying Mg/Si ratios and temperatures; Figure S7: Ethanol conversion, BD selectivity and yield for MgO-SiO_2-4 (AE) as a function of (a) GHSV and (b) contact time; Figure S8: SEM images for MgO-SiO_2-4 (AE) after reaction; Figure S9: Ethanol conversion and butadiene selectivity over MgO-SiO_2-4. Cycle 1: fresh catalyst, cycles 2 and 3: regenerated catalyst; Table S1: Density of acidic and basic sites from NH_3 and CO_2 TPD; Table S2: Density of basic and acidic sites of MgO-SiO_2-4 prepared by wet-kneading and ammonia evaporation.

Author Contributions: Formal analysis, I.B.S.; investigation, I.B.S.; writing—original draft preparation, I.B.S.; writing—review and editing, S.J. and G.-K.C.; supervision, G.-K.C.; funding acquisition, G.-K.C. All authors have read and agreed to the published version of the manuscript.

Funding: The authors acknowledge financial support from the Ministry of Education (ARC Tier 1 grant A-0004107-00-00) administered by the Faculty of Science, National University of Singapore. Ismail Bin Samsudin thanks NUS for the award of a research scholarship.

Institutional Review Board Statement: Not applicable.

Informed Consent Statement: Not applicable.

Data Availability Statement: The data presented in this study are available on request from the corresponding author.

Conflicts of Interest: The authors declare no conflict of interest.

References

1. Abdussalam-Mohammed, W.; Ali, A.; Errayes, A. Green chemistry: Principles, applications, and disadvantages. *Chem. Methodol.* **2020**, *4*, 408–423.
2. Anastas, P.T.; Zimmerman, J.B. The periodic table of the elements of green and sustainable chemistry. *Green Chem.* **2019**, *21*, 6545–6566. [CrossRef]
3. Zimmerman, J.B.; Anastas, P.T.; Erythropel, H.C.; Leitner, W. Designing for a green chemistry future. *Science* **2020**, *367*, 397–400. [CrossRef] [PubMed]
4. Sun, H.N.; Wristers, J.P. *Kirk-Othmer Encyclopedia of Chemical Technology*, 5th ed.; Wiley-Interscience: Hoboken, NJ, USA, 2004; pp. 365–392.
5. Global Butadiene Market Overview (2014–2025). Available online: https://prismaneconsulting.com/blog_details/101/Global-Butadiene-Market-Overview-(2014-2025) (accessed on 10 January 2021).
6. Morrow, N.L. The industrial production and use of 1, 3-butadiene. *Environ. Health Perspect.* **1990**, *86*, 7–8. [CrossRef]
7. White, W.C. Butadiene production process overview. *Chem. Biol. Interact.* **2007**, *166*, 10–14. [CrossRef] [PubMed]
8. Sun, H.; Wristers, J. *Kirk-Othmer Encyclopedia of Chemical Technology*, 4th ed.; Wiley-Interscience: Hoboken, NJ, USA, 2000; pp. 365–392.
9. Asia/World Energy Outlook 2013. Available online: https://eneken.ieej.or.jp/en/whatsnew/413.html (accessed on 23 January 2022).
10. Kim, S.; Jeong, S.; Heo, E. Effects of the shale boom on ethylene and propylene prices. *Energy Sources Part B Econ. Plan. Policy* **2019**, *14*, 49–66. [CrossRef]
11. Matar, S.; Hatch, L.F. *Chemistry of Petrochemical Processes*; Butterworth-Heinemann: Woburn, UK, 2001. [CrossRef]
12. Angili, T.S.; Grzesik, K.; Rödl, A.; Kaltschmitt, M. Life Cycle Assessment of Bioethanol Production: A Review of Feedstock, Technology and Methodology. *Energies* **2021**, *14*, 2939. [CrossRef]
13. Karimi, S.; Karri, R.R.; Yaraki, M.T.; Koduru, J.R. Processes and separation technologies for the production of fuel-grade bioethanol: A review. *Environ. Chem. Lett.* **2021**, *19*, 2873–2890. [CrossRef]
14. Chen, J.; Zhang, B.; Luo, L.; Zhang, F.; Yi, Y.; Shan, Y.; Liu, B.; Zhou, Y.; Wang, X.; Lü, X. A review on recycling techniques for bioethanol production from lignocellulosic biomass. *Renew. Sustain. Energy Rev.* **2021**, *149*, 111370. [CrossRef]
15. Ayodele, B.V.; Alsaffar, M.A.; Mustapa, S.I. An overview of integration opportunities for sustainable bioethanol production from first- and second-generation sugar-based feedstocks. *J. Clean. Prod.* **2020**, *245*, 118857. [CrossRef]
16. Pomalaza, G.; Ponton, P.A.; Capron, M.; Dumeignil, F.Y. Ethanol-to-butadiene: The reaction and its catalysts. *Catal. Sci. Technol.* **2020**, *10*, 4860–4911. [CrossRef]
17. Bin Samsudin, I.; Zhang, H.; Jaenicke, S.; Chuah, G. Recent Advances in Catalysts for the Conversion of Ethanol to Butadiene. *Chem. Asian J.* **2020**, *15*, 4199–4214. [CrossRef] [PubMed]
18. Kyriienko, P.I.; Larina, O.V.; Soloviev, S.O.; Orlyk, S.M. Catalytic Conversion of Ethanol Into 1,3-Butadiene: Achievements and Prospects: A Review. *Theor. Exp. Chem.* **2020**, *56*, 213–242. [CrossRef]

19. Ochoa, J.V.; Bandinelli, C.; Vozniuk, O.; Chieregato, A.; Malmusi, A.; Recchi, C.; Cavani, F. An analysis of the chemical, physical and reactivity features of $MgO–SiO_2$ catalysts for butadiene synthesis with the Lebedev process. *Green Chem.* **2016**, *18*, 1653–1663. [CrossRef]
20. Huang, X.; Men, Y.; Wang, J.; An, W.; Wang, Y. Highly active and selective binary $MgO–SiO_2$ catalysts for the production of 1, 3-butadiene from ethanol. *Catal. Sci. Technol.* **2017**, *7*, 168–180. [CrossRef]
21. Lewandowski, M.; Babu, G.S.; Vezzoli, M.; Jones, M.D.; Owen, R.E.; Mattia, D.; Plucinski, P.; Mikolajska, E.; Ochenduszko, A.; Apperley, D.C. Investigations into the conversion of ethanol to 1,3-butadiene using $MgO:SiO_2$ supported catalysts. *Catal. Commun.* **2014**, *49*, 25–28. [CrossRef]
22. Chung, S.-H.; Ramirez, A.; Shoinkhorova, T.; Mukhambetov, I.; Abou-Hamad, E.; Telalovic, S.; Gascon, J.; Ruiz-Martínez, J. The Importance of Thermal Treatment on Wet-Kneaded Silica–Magnesia Catalyst and Lebedev Ethanol-to-Butadiene Process. *Nanomaterials* **2021**, *11*, 579. [CrossRef]
23. Szabó, B.; Novodárszki, G.; Pászti, Z.; Domján, A.; Valyon, J.; Hancsók, J.; Barthos, R. $MgO–SiO_2$ Catalysts for the Ethanol to Butadiene Reaction: The Effect of Lewis Acid Promoters. *ChemCatChem* **2020**, *12*, 5686–5696. [CrossRef]
24. Reschetilowski, W.; Hauser, M.; Alscher, F.; Klauck, M.; Kalies, G. Studies on the Binary MgO/SiO_2 Mixed Oxide Catalysts for the Conversion of Ethanol to 1,3-Butadiene. *Catalysts* **2020**, *10*, 854. [CrossRef]
25. Abdulrazzaq, H.T.; Rahmani Chokanlu, A.; Frederick, B.G.; Schwartz, T.J. Reaction kinetics analysis of ethanol dehydrogenation catalyzed by $MgO–SiO_2$. *ACS Catal.* **2020**, *10*, 6318–6331. [CrossRef]
26. Chung, S.-H.; Angelici, C.; Hinterding, S.O.; Weingarth, M.; Baldus, M.; Houben, K.; Weckhuysen, B.M.; Bruijnincx, P.C. Role of Magnesium Silicates in Wet-Kneaded Silica–Magnesia Catalysts for the Lebedev Ethanol-to-Butadiene Process. *ACS Catal.* **2016**, *6*, 4034–4045. [CrossRef]
27. Zhu, Q.; Wang, B.; Tan, T. Conversion of Ethanol and Acetaldehyde to Butadiene over $MgO–SiO_2$ Catalysts: Effect of Reaction Parameters and Interaction between MgO and SiO_2 on Catalytic Performance. *ACS Sustain. Chem. Eng.* **2017**, *5*, 722–733. [CrossRef]
28. Angelici, C.; Velthoen, M.E.; Weckhuysen, B.M.; Bruijnincx, P.C.A. Influence of acid–base properties on the Lebedev ethanol-to-butadiene process catalyzed by SiO_2–MgO materials. *Catal. Sci. Technol.* **2015**, *5*, 2869–2879. [CrossRef]
29. Angelici, C.; Velthoen, M.E.Z.; Weckhuysen, B.M.; Bruijnincx, P.C.A. Effect of Preparation Method and CuO Promotion in the Conversion of Ethanol into 1,3-Butadiene over SiO_2-MgO Catalysts. *Chemsuschem* **2014**, *7*, 2505–2515. [CrossRef] [PubMed]
30. Kvisle, S.; Agüero, A.; Sneeden, R.P.A. Transformation of ethanol into 1,3-butadiene over magnesium oxide/silica catalysts. *Appl. Catal.* **1988**, *43*, 117–131. [CrossRef]
31. Niiyama, H.; Morii, S.; Echigoya, E. Butadiene Formation from Ethanol over Silica-Magnesia Catalysts. *Bull. Chem. Soc. Jpn.* **1972**, *45*, 655–659. [CrossRef]
32. Ohnishi, R.; Akimoto, T.; Tanabe, K. Pronounced catalytic activity and selectivity of $MgO–SiO_2–Na_2O$ for synthesis of buta-1, 3-diene from ethanol. *J. Chem. Soc. Chem. Commun.* **1985**, *22*, 1613–1614. [CrossRef]
33. Temuujin, J.; Okada, K.; MacKenzie, K. Role of Water in the Mechanochemical Reactions of $MgO–SiO_2$ Systems. *J. Solid State Chem.* **1998**, *138*, 169–177. [CrossRef]
34. Li, Z.; Zhang, T.; Hu, J.; Tang, Y.; Niu, Y.; Wei, J.; Yu, Q. Characterization of reaction products and reaction process of $MgO–SiO_2–H_2O$ system at room temperature. *Constr. Build. Mater.* **2014**, *61*, 252–259. [CrossRef]
35. Temuujin, J.; Okada, K.; MacKenzie, K. Formation of Layered Magnesium Silicate during the Aging of Magnesium Hydroxide-Silica Mixtures. *J. Am. Ceram. Soc.* **1998**, *81*, 754–756. [CrossRef]
36. Li, Y.; Tan, B.; Wu, Y. Ammonia-Evaporation-Induced Synthetic Method for Metal (Cu, Zn, Cd, Ni) Hydroxide/Oxide Nanostructures. *Chem. Mater.* **2008**, *20*, 567–576. [CrossRef]
37. Chen, L.-F.; Guo, P.-J.; Qiao, M.-H.; Yan, S.-R.; Li, H.-X.; Shen, W.; Xu, H.-L.; Fan, K.-N. Cu/SiO2 catalysts prepared by the ammonia-evaporation method: Texture, structure, and catalytic performance in hydrogenation of dimethyl oxalate to ethylene glycol. *J. Catal.* **2008**, *257*, 172–180. [CrossRef]
38. Li, F.; Wang, L.; Han, X.; Cao, Y.; He, P.; Li, H. Selective hydrogenation of ethylene carbonate to methanol and ethylene glycol over Cu/SiO_2 catalysts prepared by ammonia evaporation method. *Int. J. Hydrog. Energy* **2017**, *42*, 2144–2156. [CrossRef]
39. Zhu, S.; Gao, X.; Zhu, Y.; Fan, W.; Wang, J.; Li, Y. A highly efficient and robust Cu/SiO_2 catalyst prepared by the ammonia evaporation hydrothermal method for glycerol hydrogenolysis to 1,2-propanediol. *Catal. Sci. Technol.* **2015**, *5*, 1169–1180. [CrossRef]
40. Yue, H.; Zhao, Y.; Zhao, L.; Lv, J.; Wang, S.; Gong, J.; Ma, X. Hydrogenation of dimethyl oxalate to ethylene glycol on a Cu/SiO_2/cordierite monolithic catalyst: Enhanced internal mass transfer and stability. *AlChE J.* **2012**, *58*, 2798–2809. [CrossRef]
41. Toupance, T.; Kermarec, M.; Lambert, J.-F.; Louis, C. Conditions of Formation of Copper Phyllosilicates in Silica-Supported Copper Catalysts Prepared by Selective Adsorption. *J. Phys. Chem. B* **2002**, *106*, 2277–2286. [CrossRef]
42. Zhang, H.; Tan, H.-R.; Jaenicke, S.; Chuah, G.-K. Highly efficient and robust Cu catalyst for non-oxidative dehydrogenation of ethanol to acetaldehyde and hydrogen. *J. Catal.* **2020**, *389*, 19–28. [CrossRef]
43. Brew, D.; Glasser, F. Synthesis and characterisation of magnesium silicate hydrate gels. *Cem. Concr. Res.* **2005**, *35*, 85–98. [CrossRef]
44. Tonelli, M.; Martini, F.; Calucci, L.; Fratini, E.; Geppi, M.; Ridi, F.; Borsacchi, S.; Baglioni, P. Structural characterization of magnesium silicate hydrate: Towards the design of eco-sustainable cements. *Dalton Trans.* **2016**, *45*, 3294–3304. [CrossRef]

45. Pedone, A.; Palazzetti, F.; Barone, V. Models of Aged Magnesium–Silicate–Hydrate Cements Based on the Lizardite and Talc Crystals: A Periodic DFT-GIPAW Investigation. *J. Phys. Chem. C* **2017**, *121*, 7319–7330. [CrossRef]
46. Roosz, C.; Grangeon, S.; Blanc, P.; Montouillout, V.; Lothenbach, B.; Henocq, P.; Giffaut, E.; Vieillard, P.; Gaboreau, S. Crystal structure of magnesium silicate hydrates (M-S-H): The relation with 2:1 Mg–Si phyllosilicates. *Cem. Concr. Res.* **2015**, *73*, 228–237. [CrossRef]
47. Walling, S.A.; Kinoshita, H.; Bernal, S.A.; Collier, N.C.; Provis, J.L. Structure and properties of binder gels formed in the system $Mg(OH)_2$–SiO_2–H_2O for immobilisation of Magnox sludge. *Dalton Trans.* **2015**, *44*, 8126–8137. [CrossRef] [PubMed]
48. Nied, D.; Enemark-Rasmussen, K.; L'Hopital, E.; Skibsted, J.; Lothenbach, B. Properties of magnesium silicate hydrates (M-S-H). *Cem. Concr. Res.* **2016**, *79*, 323–332. [CrossRef]
49. Zhao, X.S.; Lu, G.; Whittaker, A.; Millar, G.; Zhu, H. Comprehensive study of surface chemistry of MCM-41 using 29Si CP/MAS NMR, FTIR, pyridine-TPD, and TGA. *J. Phys. Chem. B* **1997**, *101*, 6525–6531. [CrossRef]
50. Mäki-Arvela, P.; Murzin, D.Y. Effect of catalyst synthesis parameters on the metal particle size. *Appl. Catal. A Gen.* **2013**, *451*, 251–281. [CrossRef]
51. Angelici, C.; Meirer, F.; van der Eerden, A.M.J.; Schaink, H.L.; Goryachev, A.; Hofmann, J.P.; Hensen, E.J.M.; Weckhuysen, B.M.; Bruijnincx, P.C.A. Ex Situ and Operando Studies on the Role of Copper in Cu-Promoted SiO_2–MgO Catalysts for the Lebedev Ethanol-to-Butadiene Process. *ACS Catal.* **2015**, *5*, 6005–6015. [CrossRef]
52. Cornu, D.; Lin, L.; Daou, M.M.; Jaber, M.; Krafft, J.-M.; Herledan, V.; Laugel, G.; Millot, Y.; Lauron-Pernot, H. Influence of acid–base properties of Mg-based catalysts on transesterification: Role of magnesium silicate hydrate formation. *Catal. Sci. Technol.* **2017**, *7*, 1701–1712. [CrossRef]
53. Egloff, G.; Hulla, G. Conversion of Oxygen Derivatives of Hydrocarbons into Butadiene. *Chem. Rev.* **1945**, *36*, 63–141. [CrossRef]
54. Natta, G.; Rigamonti, R. *Fünfter Band: Heterogene Katalyse II*; Springer: Vienna, Austria, 1957.
55. Quattlebaum, W.M.; Toussaint, W.J.; Dunn, J.T. Deoxygenation of Certain Aldehydes and Ketones: Preparation of Butadiene and Styrene. *J. Am. Chem. Soc.* **1947**, *69*, 593–599. [CrossRef]
56. Arundale, E.; Mikeska, L.A. The Olefin-Aldehyde Condensation. The Prins Reaction. *Chem. Rev.* **1952**, *51*, 505–555. [CrossRef]
57. Sushkevich, V.L.; Ivanova, I.I. Ag-Promoted ZrBEA Zeolites Obtained by Post-Synthetic Modification for Conversion of Ethanol to Butadiene. *Chemsuschem* **2016**, *9*, 2216–2225. [CrossRef] [PubMed]
58. Pomalaza, G.; Capron, M.; Ordomsky, V.; Dumeignil, F. Recent Breakthroughs in the Conversion of Ethanol to Butadiene. *Catalysts* **2016**, *6*, 203. [CrossRef]
59. Makshina, E.; Janssens, W.; Sels, B.; Jacobs, P.A. Catalytic study of the conversion of ethanol into 1,3-butadiene. *Catal. Today* **2012**, *198*, 338–344. [CrossRef]
60. Li, S.; Men, Y.; Wang, J.; Liu, S.; Wang, X.; Ji, F.; Chai, S.; Song, Q. Morphological control of inverted MgO-SiO_2 composite catalysts for efficient conversion of ethanol to 1, 3-butadiene. *Appl. Catal. A* **2019**, *577*, 1–9. [CrossRef]
61. Chieregato, A.; Velasquez Ochoa, J.; Bandinelli, C.; Fornasari, G.; Cavani, F.; Mella, M. On the Chemistry of Ethanol on Basic Oxides: Revising Mechanisms and Intermediates in the Lebedev and Guerbet reactions. *ChemSusChem* **2015**, *8*, 377–388. [CrossRef] [PubMed]
62. Janssens, W.; Makshina, E.V.; Vanelderen, P.; De Clippel, F.; Houthoofd, K.; Kerkhofs, S.; Martens, J.A.; Jacobs, P.A.; Sels, B.F. Ternary Ag/MgO-SiO_2 Catalysts for the Conversion of Ethanol into Butadiene. *Chemsuschem* **2015**, *8*, 994–1008. [CrossRef]
63. Natta, G.; Rigamonti, R. *Sintesi Del Butadiene Da Alcool Etilico*; La Chimica e l'Industria: Milan, Italy, 1947; pp. 195–200.
64. Yan, T.; Yang, L.; Dai, W.; Wang, C.; Wu, G.; Guan, N.; Hunger, M.; Li, L. On the deactivation mechanism of zeolite catalyst in ethanol to butadiene conversion. *J. Catal.* **2018**, *367*, 7–15. [CrossRef]
65. Taifan, W.E.; Li, Y.; Baltrus, J.P.; Zhang, L.; Frenkel, A.I.; Baltrusaitis, J. Operando structure determination of Cu and Zn on supported MgO/SiO_2 catalysts during ethanol conversion to 1, 3-butadiene. *ACS Catal.* **2018**, *9*, 269–285. [CrossRef]
66. Zhang, M.; Qin, Y.N.; Tan, X.; Wang, L.; Yu, Y.; Jiang, H. Study of ethanol/acetaldehyde to 1, 3-butadiene over MgO–SiO_2 catalyst: Comparative investigation of deactivation behaviour due to carbon deposition. *Catal. Lett.* **2020**, *150*, 1462–1470. [CrossRef]
67. Chae, H.-J.; Kim, T.-W.; Moon, Y.-K.; Kim, H.-K.; Jeong, K.-E.; Kim, C.-U.; Jeong, S.-Y. Butadiene production from bioethanol and acetaldehyde over tantalum oxide-supported ordered mesoporous silica catalysts. *Appl. Catal. B Environ.* **2013**, *150–151*, 596–604. [CrossRef]